1 of 1

Rose McCallen
Engineer

Phil Gresho
Scientist

John Leone
Meteorologist

Lawrence Livermore National Laboratory
University of California
Livermore, CA 94551

Wolfgang Kollmann
Professor
University of California, Davis
Davis, CA 95616

LARGE-EDDY SIMULATION USING THE FINITE ELEMENT METHOD

A large-eddy simulation for the modeling of turbulent flow is used in conjunction with the finite element method. This approach is shown to accurately predict the transient, complex flow over a two-dimensional backward-facing step at a Reynolds number of 10,000. The instantaneous and time-averaged results from the large-eddy simulation are evaluated by comparison to a direct numerical simulation.

Introduction

In a large-eddy simulation (LES) of turbulent flows, the large-scale motion is calculated explicitly (i.e., resolved) and the small-scale motion is modeled (i.e., approximated with semi-empirical relations). Typically, finite difference or spectral numerical schemes are used to generate an LES; the use of finite element methods (FEM) has been far less prominent.

Only three publications were found in the open literature where an LES was computed using FEM (Kondo et al., 1986, Findikakis et al., 1978, and Findikakis and Street, 1980). Kondo et al. (1986) successfully simulated the coupled fluid/structure problem of turbulent flow past an elastic shell. Findikakis et al. (1978) and Findikakis and Street (1980) simulated turbulent stratified flows with a free surface representing flow in reservoirs, lakes, or estuaries.

In this study, we demonstrate that FEM in combination with LES provides a viable tool for the study of turbulent, separating channel flows, specifically the flow over a two-dimensional backward-facing step. The combination of these methodologies brings together the advantages of each: LES provides a high degree of accuracy with a minimum of empiricism for turbulence modeling and FEM provides a robust way to simulate flow in very complex domains of practical interest. Such a combination should prove very valuable to the engineering community.

Governing Equations

The LES averaging of the instantaneous velocity for all the turbulent motions, u_α, filters out the small-scale motions, u'_α, and results in the instantaneous velocity for only the large-scale motions, $\overline{u_\alpha}$, such that $u_\alpha = \overline{u_\alpha} + u'_\alpha$. The overbar represents a filtering operator (Kwak et al., 1975). The small-scale motions which are modeled are referred to as the subgrid-scale (SGS) motion or residual field.

For a finite domain, the resolved field can be defined by cell volume-averaging;

$$\overline{u_\alpha}(\underline{x},t) = \frac{1}{\Delta}\int_{x_1-\frac{1}{2}\Delta x_1}^{x_1+\frac{1}{2}\Delta x_1}\int_{x_2-\frac{1}{2}\Delta x_2}^{x_2+\frac{1}{2}\Delta x_2}\int_{x_3-\frac{1}{2}\Delta x_3}^{x_3+\frac{1}{2}\Delta x_3} u_\alpha(\underline{x}',t)\,d\underline{x}' \qquad (1)$$

where $\Delta = (\Delta x_1 \Delta x_2 \Delta x_3)^{1/3}$ is the filter size.

The filtered incompressible Navier-Stokes equations are

$$\frac{\partial \overline{u_\alpha}}{\partial x_\alpha} = 0 \qquad (2)$$

$$\frac{\partial \overline{u_\alpha}}{\partial t} + \overline{u_\beta}\frac{\partial \overline{u_\alpha}}{\partial x_\beta} = \frac{\partial \overline{\tau_{\alpha\beta}}}{\partial x_\beta} \qquad (3)$$

where the pseudo stress term[1] is

$$\overline{\tau_{\alpha\beta}} = -\overline{P}\delta_{\alpha\beta} + \upsilon\frac{\partial \overline{u_\alpha}}{\partial x_\beta} - (L_{\alpha\beta} + C_{\alpha\beta} + R_{\alpha\beta}) \qquad (4)$$

and

$$\overline{P} = \frac{\overline{p}}{\rho} + \frac{1}{3}\delta_{\alpha\beta}\overline{u'_\gamma u'_\gamma}$$

---

[1]Need $\upsilon\left(\partial\overline{u_\alpha}/\partial x_\beta + \partial\overline{u_\beta}/\partial x_\alpha\right)$ for correct/true viscous term.

$$L_{\alpha\beta} = \overline{\overline{u_\alpha}\,\overline{u_\beta}} - \overline{u_\alpha}\,\overline{u_\beta}$$

$$C_{\alpha\beta} = \overline{\overline{u_\alpha}\,\overline{u_\beta}} + \overline{\overline{u_\alpha}\,u_\beta}$$

$$R_{\alpha\beta} = \overline{u_\alpha u_\beta} - \frac{1}{3}\delta_{\alpha\beta}\overline{u_\gamma u_\gamma} \quad .$$

The terms $C_{\alpha\beta}$ and $R_{\alpha\beta}$ in (4), representing the small-scale motion, are the nonclosed terms that must be modeled by using what is typically called an SGS model. Following, e.g., Deardorff (1970), we make the simplification here that $C_{\alpha\beta} = 0$, and thus, only $R_{\alpha\beta}$ remains to be modeled. The term $L_{\alpha\beta}$ can be solved explicitly. For the numerical approached used here (i.e., one-point Gaussian quadrature and cell volume-averaging over an element) we have $L_{\alpha\beta} = 0$ (McCallen, 1993).

The weak forms obtained via (2) and (3) for the domain Ω are

$$\int_\Omega w \frac{\partial \overline{u_\alpha}}{\partial x_\alpha} = 0 \tag{5}$$

$$\int_\Omega v\left(\frac{\partial \overline{u_\alpha}}{\partial t} + \overline{u_\beta}\frac{\partial \overline{u_\alpha}}{\partial x_\beta}\right) - \int_\Omega v\frac{\partial \overline{\tau_{\alpha\beta}}}{\partial x_\beta} = 0 \tag{6}$$

where w and v are appropriate sets of test functions. Integrating the stress term in (6) by parts and applying the divergence theorem, we arrive at the final weak form

$$\int_\Omega\left[v\left(\frac{\partial \overline{u_\alpha}}{\partial t} + \overline{u_\beta}\frac{\partial \overline{u_\alpha}}{\partial x_\beta}\right) + \left(\upsilon\frac{\partial \overline{u_\alpha}}{\partial x_\beta} - \overline{P} - R_{\alpha\beta}\right)\frac{\partial v}{\partial x_\beta}\right] = \int_{\partial\Omega} v f_\alpha \tag{7}$$

where $f_\alpha = n_\beta \overline{\tau_{\alpha\beta}}$, is the (user-supplied) natural boundary condition, $\partial\Omega$ is the boundary surface, and n_β is the surface outward normal in the β-direction. In this formulation, the natural boundary condition includes the small-scale motion.

The velocity components $\overline{u_\alpha}$ and pressure $\overline{P}$ are expanded into the appropriate basis functions ϕ_j and ψ_j as follows:

$$\overline{u_\alpha}^h(\underline{x},t) = \sum_{j=1}^{N} \overline{u_\alpha}^j(t)\ \phi_j(\underline{x}) \tag{8}$$

$$\overline{P}^h(\underline{x},t) = \sum_{j=1}^{M} \overline{P}^j(t)\ \psi_j(\underline{x}) \tag{9}$$

where N is the total number of velocity basis functions and M is the total number of pressure basis functions. The superscript h signifies that $\overline{u_\alpha}^h$ and $\overline{P}^h$ are the approximate weak solutions on a discretization of the computational domain (with characteristic element size h). These approximate solutions are defined continuously at all points in the flow field, not just at discrete points as with finite difference schemes. The basis functions define the spatial variation of the solutions.

Substituting the expansions (8) and (9) into (5) and (7) and setting $v = \phi_i$ and $w = \psi_i$ (i.e., the Galerkin finite element method), we have

$$\left(\int_\Omega \psi_i \frac{\partial \phi_j}{\partial x_\alpha}\right)\overline{u_\alpha}^j = 0 \tag{10}$$

$$\left(\int_\Omega \phi_i\phi_j\right)\frac{\partial \overline{u_\alpha}^j}{\partial t} + \left(\overline{u_\beta}^k \int_\Omega \phi_i\phi_k \frac{\partial \phi_j}{\partial x_\beta}\right)\overline{u_\alpha}^j + \left(\int_\Omega \upsilon \frac{\partial \phi_i}{\partial x_\beta}\frac{\partial \phi_j}{\partial x_\beta}\right)\overline{u_\alpha}^j - \left(\int_\Omega \psi_j \frac{\partial \phi_i}{\partial x_\alpha}\right)\overline{P}^j - \left(\int_\Omega R_{\alpha\beta}\frac{\partial \phi_i}{\partial x_\beta}\right)\overline{u_\alpha}^j = \int_{\partial\Omega}\phi_i f_\alpha \tag{11}$$

where summation over j and k is now implied. The form of the nonclosed SGS terms depends on the SGS model.

Subgrid-Scale Model

For the initial demonstration, we considered only two-dimensional problems to reduce the computational resources required for the study. Thus, we formulated the continuous model equations using two-dimensional turbulence theory. The vorticity model developed by Leith (1969) for two-dimensional LES was employed for the SGS model.

Following Smagorinsky (1963), we set

$$R_{\alpha\beta} = \overline{u_\alpha u_\beta} - \frac{1}{3}\delta_{\alpha\beta}\overline{u_\gamma u_\gamma} = -2\upsilon_T S_{\alpha\beta} \tag{12}$$

where

$$S_{\alpha\beta} \equiv \frac{1}{2}\left(\frac{\partial \overline{u}_\alpha}{\partial x_\beta} + \frac{\partial \overline{u}_\beta}{\partial x_\alpha}\right)$$

and υ_T is the eddy viscosity coefficient. Leith (1969) developed a vorticity relation for υ_T in two dimensions which accounts for the -3 power spectrum and the enstrophy cascade to small scales in two-dimensional simulations. (Enstrophy is defined as one-half the square of the vorticity, $\omega^2/2$.) Using dimensional analysis coupled with

Smagorinsky's procedure, Leith (1969) shows that if the truncation wave number k_c lies within a -3 power spectrum, the eddy viscosity coefficient is proportional to k_c^{-3} (or Δ^3). The derived vorticity relation for the eddy viscosity coefficient is

$$\upsilon_T = (c_\omega \Delta)^3 |\nabla \omega| \tag{13}$$

where $\nabla\omega$ is defined by Leith (1969) as "the finite difference approximation to the vorticity gradient" and c_ω is a constant.

In two dimensions, where the resolved or large-scale vorticity is $\bar{\omega} = \frac{\partial \bar{u}_2}{\partial x_1} - \frac{\partial \bar{u}_1}{\partial x_2}$, we have

$$|\nabla\omega| = \left[\left(\frac{\partial \bar{\omega}}{\partial x_1}\right)^2 + \left(\frac{\partial \bar{\omega}}{\partial x_2}\right)^2\right]^{1/2}$$

$$= \left[\left(\frac{\partial^2 \bar{u}_2}{\partial x_1^2} - \frac{\partial^2 \bar{u}_1}{\partial x_1 \partial x_2}\right)^2 + \left(\frac{\partial^2 \bar{u}_2}{\partial x_1 \partial x_2} - \frac{\partial^2 \bar{u}_1}{\partial x_2^2}\right)^2\right]^{1/2}. \tag{14}$$

Numerical Method

The discretized continuity and momentum equations (10) and (11) can be written in matrix form

$$C^T \bar{u} = 0 \tag{15}$$

$$M\dot{\bar{u}} + \left[K + N(\bar{u})\right]\bar{u} + C\bar{P} = F \tag{16}$$

where $\bar{u}$ is the nodal velocity vector, $\bar{P}$ is the pressure vector, and in three-dimensional space, after substituting the SGS model,

$$M = \begin{bmatrix} m_{ij} & 0 & 0 \\ 0 & m_{ij} & 0 \\ 0 & 0 & m_{ij} \end{bmatrix}, \quad m_{ij} = \int_\Omega \phi_i \phi_j$$

$$K = \begin{bmatrix} k_{ij_{(11)}} & k_{ij_{(12)}} & k_{ij_{(13)}} \\ k_{ij_{(21)}} & k_{ij_{(22)}} & k_{ij_{(23)}} \\ k_{ij_{(31)}} & k_{ij_{(32)}} & k_{ij_{(33)}} \end{bmatrix},$$

$$k_{ij_{(\alpha\beta)}} = \int_\Omega \left(\delta_{\alpha\beta}\left(\upsilon + \upsilon_T^h\right)\left(\frac{\partial \phi_i}{\partial x_\gamma}\frac{\partial \phi_j}{\partial x_\gamma}\right) + \upsilon_T^h \frac{\partial \phi_j}{\partial x_\alpha}\frac{\partial \phi_i}{\partial x_\beta} \right)$$

$$N = \begin{bmatrix} n_{ij}(\bar{u}) & 0 & 0 \\ 0 & n_{ij}(\bar{u}) & 0 \\ 0 & 0 & n_{ij}(\bar{u}) \end{bmatrix},$$

$$n_{ij}(\bar{u}) = \overline{u}_\beta^k \int_\Omega \phi_i \phi_k \frac{\partial \phi_j}{\partial x_\beta}$$

$$C = \begin{bmatrix} c_{ij_{(1)}} \\ c_{ij_{(2)}} \\ c_{ij_{(3)}} \end{bmatrix}, \quad c_{ij_{(\alpha)}} = -\int_\Omega \psi_j \frac{\partial \phi_i}{\partial x_\alpha}$$

$$C^T = \begin{bmatrix} c_{j_{i(1)}} & c_{j_{i(2)}} & c_{j_{i(3)}} \end{bmatrix}, \quad c_{j_{i(\alpha)}} = -\int_\Omega \psi_i \frac{\partial \phi_j}{\partial x_\alpha}$$

$$F = \begin{bmatrix} f_{i_{(1)}} \\ f_{i_{(2)}} \\ f_{i_{(3)}} \end{bmatrix}, \quad f_{i_{(\alpha)}} = \int_\Omega \phi_i f_\alpha$$

where υ_T^h for the two-dimensional case is the eddy viscosity defined by the vorticity model (13) with the expansion (8) substituted for the velocities.

In the current study, the discrete Poisson equation for pressure is solved in place of the continuity equation (15), so that continuity and momentum are decoupled and an explicit time-integration scheme is used. The discrete Poisson equation for pressure is an approximation of the continuous Poisson equation. The continuous Poisson equation is derived by taking the divergence of the momentum equation and applying the continuity equation, $\nabla \cdot \bar{u} = 0$. The analogous discrete Poisson equation is derived by multiplying the matrix form of the momentum equation (16) by $C^T M^{-1}$, and since and $d\,C^T \bar{u} / dt = 0$, we obtain

$$C^T M^{-1} C \bar{P} = C^T M^{-1}\left[(K + N(\bar{u}))\,\bar{u} - F\right] \tag{17}$$

where the coefficient matrix $C^T M^{-1} C$ is a discrete approximation of the Laplacian operator. Thus, the final spatially discretized equations in matrix form are (16) and (17).

To reduce computational cost, a lumped mass matrix M is employed and the coefficient matrices are generated using reduced order integration based on one-point Gaussian quadrature. The coefficient calculations are performed at the element level using isoparametric quadrilateral elements with bi-linear basis functions for the velocity expansion and piecewise-constant basis functions for the pressure expansion. The element contributions are then added to form the global matrices using standard

FEM assembly techniques. The pressure Poisson equation (17) is solved directly with a skyline solver (one back substitution per time step of the previously factored matrix) and an explicit forward Euler time integration scheme is used for the velocity solution.

Balancing tensor diffusivity (BTD) is a technique for applying an additive diffusivity (correction) to the diffusion matrix which balances the negative diffusion caused by the explicit Euler time integration (Gresho et al., 1984). This correction is applied at the element level at each time step.

When one-point quadrature is used, zero energy modes may be present (Gresho et al., 1984). These zero energy modes are undiffused 'waves' that are null vectors of the diffusion matrix. In two dimensions, there is one $2\Delta x$ by $2\Delta y$ wave, which has alternating nodal values of ± 1. To insure diffusion of these waves, an hour-glass correction matrix is added to the one-point quadrature diffusion matrix (Goudreau and Hallquist, 1982 and Gresho et al., 1984).

The solution of the advection term $n_{ij}(\bar{u})$ can be expensive because of the integration of a triple product. To reduce the triple product to a double product, Gresho et al. (1984) suggest a simplification using what they term a 'centroid advection velocity', in which, at the element level

$$\overline{u}^{k}_{\beta_e} \equiv \left[\sum_{k=1}^{N} \overline{u}^{k}_{\beta_e} \phi_k \right]_{centroid\ of\ \Omega_e}$$

where N is the number of nodes per element. We employ this simplification in (16) and (17).

Boundary Conditions

To simulate the wall region 'exactly' requires the specification of a no-slip boundary condition, very fine discretization of the region, *and* the equations of motion must account for the low Reynolds-number flow close to the wall (e.g., the SGS stresses should asymptotically go to zero at the wall). The Stanford group (Moin et al., 1978, Moin and Kim, 1981, Spalart, 1988) have simulated wall regions as accurately as possible for simple (nonseparating) flows. However, most researchers applying LES to more complicated geometries utilize wall models (artificial boundary conditions) to represent the physics in the region close to the wall (Deardorff 1970, Schumann 1975, Mason and Callen 1986). This is usually done by setting the instantaneous stress at the wall proportional to the tangential velocity at the first grid point away from the wall. The coefficient of proportionality can be described by either a logarithmic, power, or linear law-of-the-wall relation depending on the type of flow simulation and location of the first grid point relative to the wall. The normal velocity component at the wall is set to zero. With LES, the approximate boundary conditions must be applied everywhere on a plane surface parallel to the wall and are time dependent.

Piomelli et al. (1987) has provided a detailed review of wall models used in LES's by past researchers for nonseparating flows. However, for high Reynolds-number flows with separation, the results of past research do not provide guidance or consensus on wall modeling. The commonly used law-of-the-wall approximations are accurately known only for two-dimensional geometries and then only for steady attached flows. For example, Ruderich and Fernholz (1986) have shown that for flows with separation, reverse flow, and reattachment, the near-wall flow does not follow a logarithmic law-of-the-wall. Reynolds (1989) also states that assuming that the law-of-the-wall is satisfied instantaneously is 'an unlikely assumption'.

A plausible option is to use the LES approach all the way to the wall *without* resolving the wall region. In other words, an SGS model is used even for the elements in the wall region. This implies that the small-scale motion at the wall (i.e., motion that is smaller than the resolved scale) is the same as, or at least similar to, the small-scale motion away from the wall. This seems to be a reasonable assumption, especially for the shedding vortices of a backward-facing step, where the wall region and the core flow are similar (i.e., the grid-size eddies at the walls are similar to eddies away from the walls).

It is clear from the above brief review that the use of wall models for separated flows in conjunction with the LES approach is still under development. In the current work, it would be preferable to resolve the wall region, but this would require excessive computer resources. Instead, the above described approach of using the SGS model also in the wall region is utilized in the current work.

Results

Our test bed problem was the two-dimensional, backward-facing step problem at a Reynolds number of 10,000 (based on the inlet velocity and two times the inlet channel height). The problem geometry was a channel of unit height with a step height of 0.5 and a total channel length of 10.0 channel heights. The computational domain begins at the step with a nearly flat inflow velocity profile of 1.0 specified at the step. The boundary

conditions used were no-penetration and no-slip at the walls, and homogeneous natural boundary conditions at the outflow. The vorticity model constant $c_\omega = (0.1)^{2/3} = 0.2154$. (The value 0.1 is typically used for the Smagorinsky SGS model constant c for three-dimensional simulations, and we appropriately set $c_\omega = (c)^{2/3}$ (Findikakis, 1980)).

Because we have chosen a two-dimensional problem where $\overline{u}_3 = 0$ and $\partial/\partial x_3 = 0$ by construction, it is impossible to compare our numerical results to experimental results which are three-dimensional with significant velocities and gradients in the third dimension. Therefore, in order to validate our results for this numerical experiment, we first completed a direct numerical simulation (DNS) of the test problem using the Navier-Stokes portion of the same code (i.e., omitting the $R_{\alpha\beta}$ term in (11)). A series of mesh refinement studies showed that a simulation using a uniform 100x1000 element mesh and a time step of 0.005 resolves virtually all relevant scales.

The DNS showed a complicated time-varying flow with vortices shedding off both the step and top wall and propagating downstream. The simulation went through a transient and then developed a periodic solution which we used for verification of the LES results. We believe that the periodic solution was a result, in part, of not perturbing the inflow velocity field.

The DNS should be filtered (i.e., cell volume-averaged) for comparison to the LES. However, we found that the filtered DNS varied only slightly from the unfiltered DNS (McCallen, 1993). Thus, in the current study the DNS was directly compared to the LES.

Although we have obtained LES results on a number of different mesh densities and configurations (McCallen, 1993), we will report the results obtained on a 32x244 element graded mesh. This mesh was uniform in the core of the flow and graded in the wall regions. A 6 to 1 mesh grading was used for the 6 elements closest to the walls. To demonstrate the ability of LES to represent the large-scale phenomena, we present in Fig. 1 a series of snapshots of the stream function from both the LES and the DNS over one shedding period. A comparison of these figures illustrates that the LES captures the vortex shedding off both the step and the upper wall with great fidelity. The downstream propagation of the vortices is also well represented. The propagation speed in the LES simulation is only 1% higher than that in the DNS. We have also examined velocity time histories for several nodes. While the small-scale details of the behavior at a single point in the flow field are not particularly well represented (Figs. 2 and 3), the large-scale features are represented well. For example, at $(x_1, x_2) = (2.0, 0.25)$ the oscillation period of $\overline{u}_1$ for the LES is within 1% of the DNS period. Also, power spectra calculated from these time histories show that LES is predicting the correct dominant frequencies (Figs. 4 and 5).

A profile plot at one snapshot in time (Fig. 6) shows the variation of υ_T in the cross-stream direction. Corresponding profile plots of vorticity for the same snapshot in time are shown in Fig. 7. The magnitude of υ_T is less than three times the *molecular* viscosity, υ. These results also indicate that the SGS model contribution is the same order of magnitude as the molecular diffusion term.

The velocity profiles near the channel outlet for a snapshot in time (Fig. 8) are smooth in the cross-stream direction and vary smoothly as we move upstream. This implies that the zero natural boundary condition at the channel outlet is a useful outlet condition. The natural boundary condition is defined by our equation formulation, and in our formulation, it includes the SGS motion (see equations (4) and (7)).

In addition to the analysis of the transient results, we also compared time-averaged results for the reattachment length of the major recirculation zone. The reattachment length for the DNS was 3.4 step heights while the LES results gave a length of 3.1 step heights, or 9% shorter. The reattachment lengths for these two-dimensional simulations are not expected to compare with experimental results which are inherently three-dimensional. The LES time-averaged $\overline{u}_1$ velocity at selected locations are shown in Fig. 9 along with the associated streamline plot for the time-averaged velocity.

To clearly show the improvement in the solution by the addition of the SGS model, we next present results for the 32x244 mesh without the SGS model (i.e., a direct numerical simulation). The time histories in Figs. 10 and 11 show that the DNS with the 32x244 mesh are not periodic and do not compare well to the DNS with a 100x1000 mesh. Also, the predicted velocities for the DNS with the 32x244 mesh showed wiggles in the wall region whereas wiggles were not present when the SGS model was used with the same mesh. Therefore, even though the SGS model contribution is small (i.e., the υ_T values are comparable in magnitude to the molecular viscosity), it successfully stabilizes

the calculations and provides an accurate solution at a significant reduction in computational effort.

Conclusions

These results show that the LES/FEM approach to simulating turbulent flows around complex geometries has potential as an efficient and effective method. For the case presented here the combination of LES with FEM and a graded mesh produced an accurate simulation of the large-scale flow using only 7,808 elements in comparison to 100,000 elements needed for the DNS. While this work must be extended to more complex problems and to three-dimensions before a final judgment can be made, we feel that LES/FEM shows great promise as a tool for analyzing turbulent flows in complex geometry.

Acknowledgment

Computer time allocations from the National Supercomputing Center for Energy and the Environment (NSCEE) at the University of Nevada, Las Vegas and from the National Energy Research Supercomputer Center (NERSC) at LLNL are gratefully acknowledged.

This work was performed under the auspices of the U.S. Department of Energy by Lawrence Livermore National Laboratory under Contract W-7405-Eng-48.

References

Deardorff, J.W., 1970, "A Numerical Study of Three-Dimensional Turbulent Channel Flow at Large Reynolds Numbers," *J. of Fluid Mech.*, **41**, Part 2, pp. 453-480.

Findikakis, A.N., 1980, "Finite Element Simulation of Turbulent Stratified Flows," Dissertation, Stanford University, Department of Civil Engineering.

Findikakis, A.N. and Street, R.L., 1980, "Numerical Simulation of Turbulent Stratified Flows in Surface Water Impoundments," Proc. of the Spec. Conf. on Comput. and Phys. Model in Hydraul. Eng., Chicago, Illinois, August 6-8, 1980, Published by ASCE, New York, NY pp. 249-260.

Findikakis, A.N., Franzini, J.B., and Street, R.L., 1978, "Simulation of Stratified Turbulent Flows in Closed Water Bodies Using the Finite Element Method," Proceedings from Finite Elements in Water Resources Conference, July 1978, London, England, pp. 3/23-44.

Goudreau, G. and Hallquist, J., 1982, "Recent Developments in Large-Scale Finite Element Lagrangian Hydrocode Technology," *Comp. Meth. Appl. Mech. Eng.*, **33**, p.725.

Gresho, P.M., Chan, S.T., Lee, R.L., and Upson, C.D., 1984, "A Modified Finite Element Method for Solving the Time-Dependent Incompressible Navier-Stokes Equations. Part 1: Theory," *Int. J. Num. Meth. in Fluids*, **4**, pp. 557-598.

Kondo, N., Tosaka, N., and Nishimura, T., 1986, "Finite Element Analysis for Turbulent Flows - Elastic Shell Interaction," Proceedings from Sixth International Symposium on Finite Element Methods in Flow Problems, 16-20 June 1986, Antibes, France, pp. 177-181.

Kwak, D., Reynolds, W.C., and Ferziger, J.H., 1975, "Three Dimensional Time Dependent Computation of Turbulent Flow," Report No. TF-5, Stanford University, Department of Mechanical Engineering.

Leith, C.E., 1969, "Numerical Simulation of Turbulent Flow," in *Properties of Matter under Unusual Conditions*, H. Mark and S. Ferback eds., Interscience.

Mason, P.J. and Callen, N.S., 1986, "On the Magnitude of the Subgrid-Scale Eddy Coefficient in Large-Eddy Simulation of the Turbulent Channel Flow," *J. Fluid Mech.*, **162**, pp. 439-462.

McCallen, R., 1993, "Large-Eddy Simulation of Turbulent Flow Using the Finite Element Method," Ph.D. Thesis, University of California, Davis.

Moin, P. and Kim, J.J., 1981, "Numerical Investigation of Turbulent Channel Flow," *J. Fluid Mech.*, **118**, pp. 341-377.

Moin, P., Reynolds, W.C., and Ferziger, J.H., 1978, "Large Eddy Simulation of Turbulent Channel Flow," Report No. TF-12, Stanford University, Department of Mechanical Engineering.

Piomelli, U., Ferziger, J.H., and Moin P., 1987, "Models for Large Eddy Simulations of Turbulent Channel Flows including Transpiration," Report No. TF-32, Stanford University, Department of Mechanical Engineering.

Reynolds, W.C., 1989, "The Potential and Limitations of Direct and Large Eddy Simulations," Position paper, Whither Turbulence Workshop, Cornell University, March 22-24, pp. 1-30.

Ruderich, R. and Fernholz, H.H., 1986, "An Experimental Investigation of a Turbulent Shear Flow with Separation, Reverse Flow, and Reattachment," *J. of Fluid Mech.*, **163**, pp. 283-322.

Schumann, U., 1975, "Subgrid Scale Model for Finite Difference Simulations of Turbulent Flows in Plane Channels and Annuli," *J. of Computational Physics*, **18**, p. 376-404.

Smagorinsky, J., 1963, "General Circulation Experiments with the Primitive Equations, I. The

Basic Experiment," *Monthly Weather Review*, **91**, No. 3, pp. 99-164.

Spalart, P.R. 1988, "Direct Numerical Simulation of a Turbulent Boundary Layer up to R_e=1410," *J. Fluid Mech.*, **187**, p. 61.

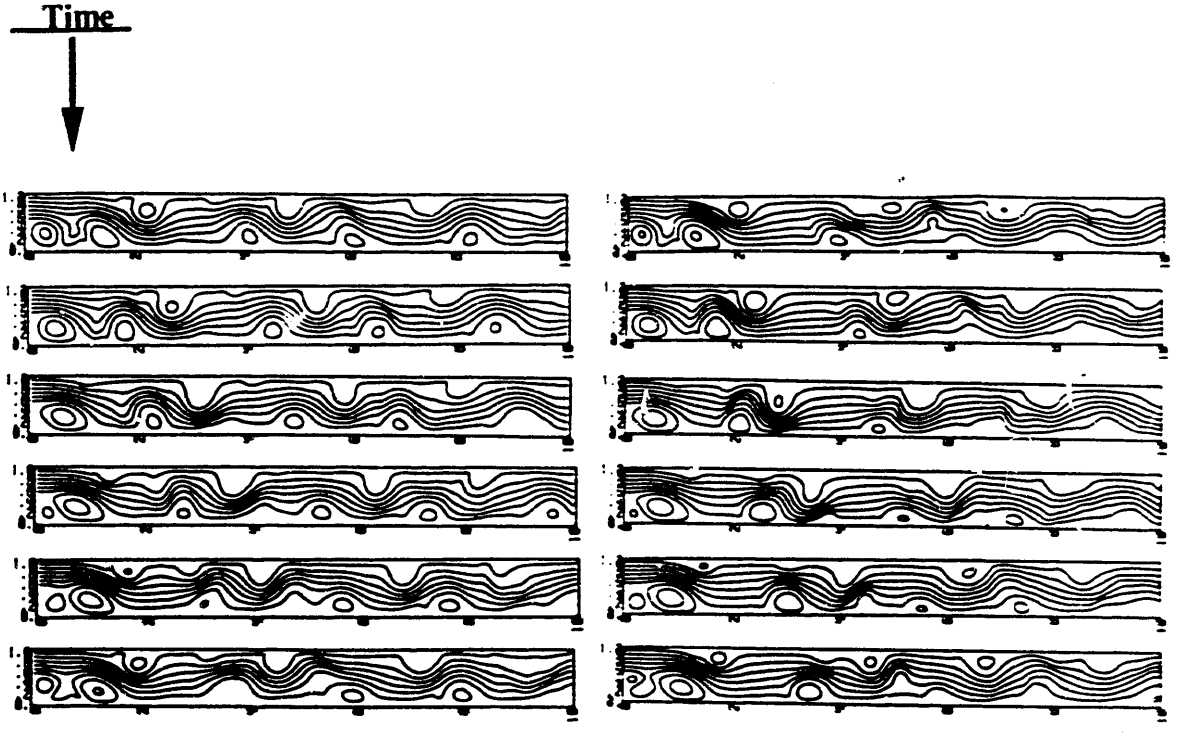

LES with 32 x 244 Mesh **Direct Numerical Simulation**

Fig. 1. Time series of stream function plots for the LES and DS. (One period is shown for the same specified stream function levels for each case at 0, 1/6, 2/6, 3/6, 4/6, and 5/6 of a DNS period.)

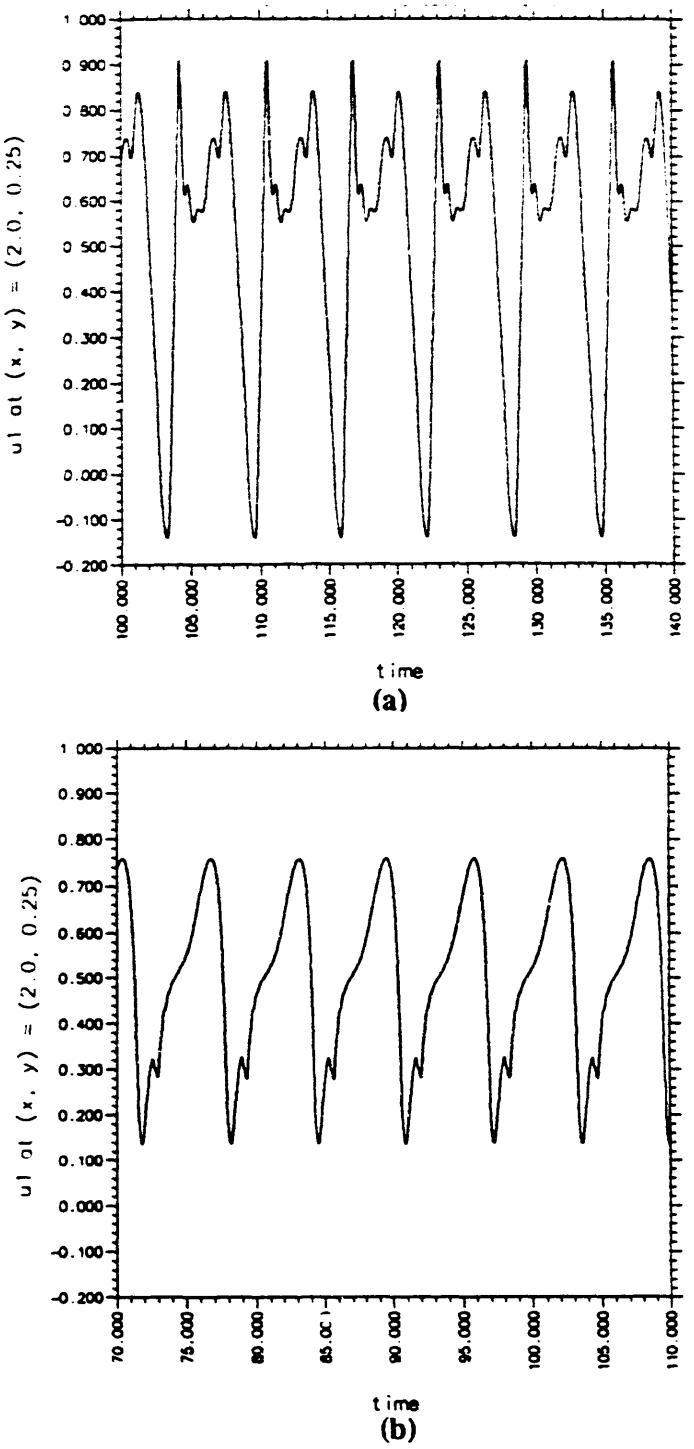

Fig. 2. Time histories of $\overline{u_1}$ at $(x_1, x_2) = (2.0, 0.25)$ for a) the LES 32x244 mesh and b) the DNS (shown for the same axis scale).

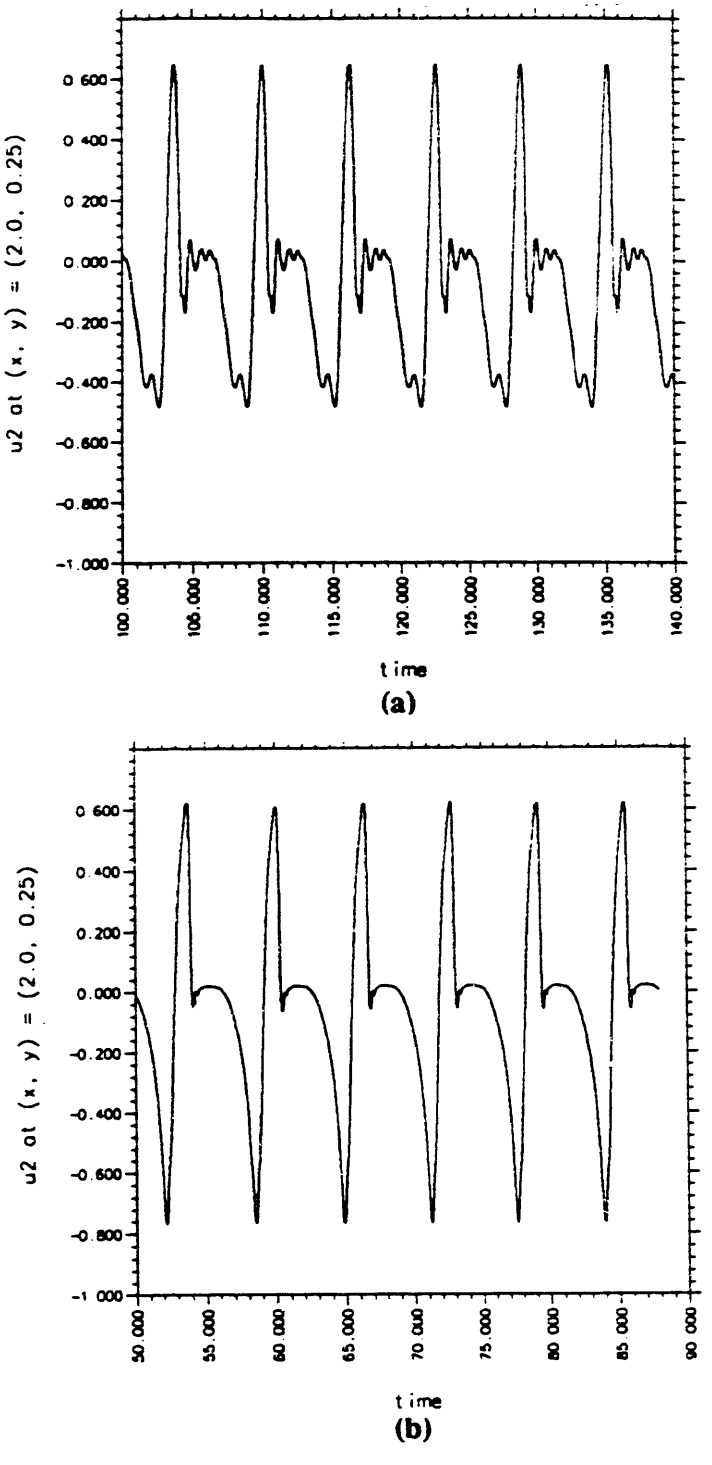

Fig. 3. Time histories of $\overline{u_2}$ at $(x_1, x_2) = (2.0, 0.25)$ for a) the LES 32x244 mesh and b) the DNS (shown for the same axis scale).

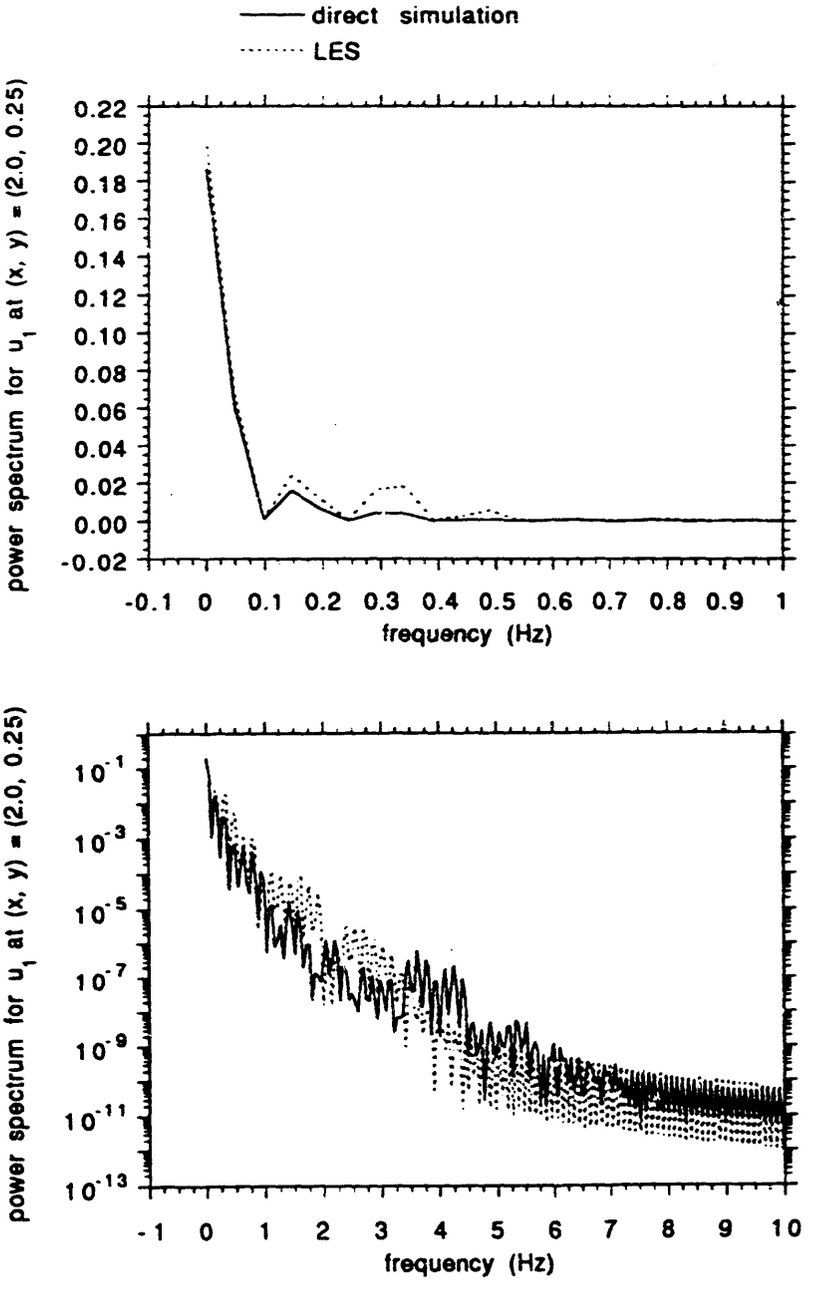

Fig. 4. Power spectrum for $\overline{u_1}$ at $(x_1, x_2) = (2.0, 0.25)$ for the LES and DNS. (Plots for linear and log ordinate axis are shown.)

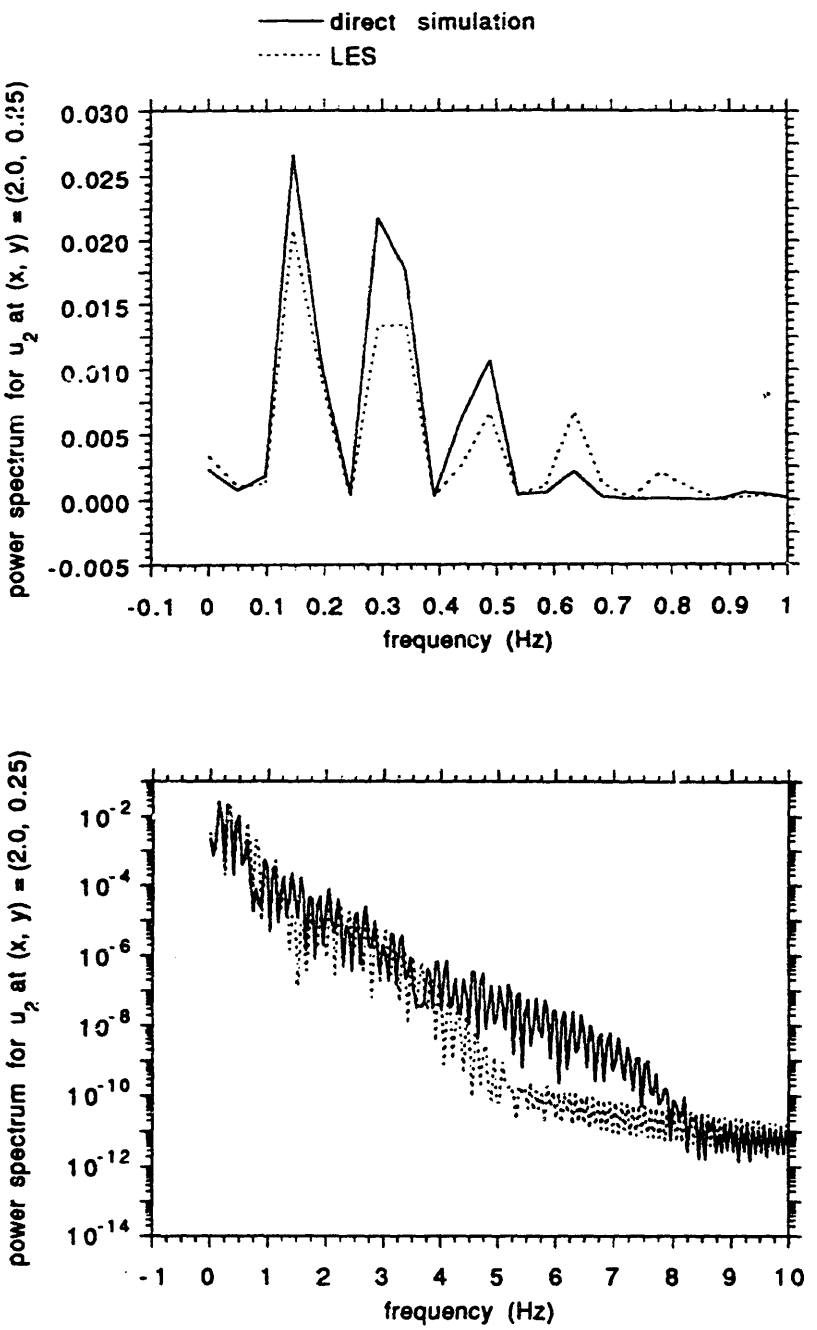

Fig. 5. Power spectrum for $\overline{u_2}$ at $(x_1, x_2) = (2.0, 0.25)$ for the LES and DNS. (Plots for linear and log ordinate axis are shown.)

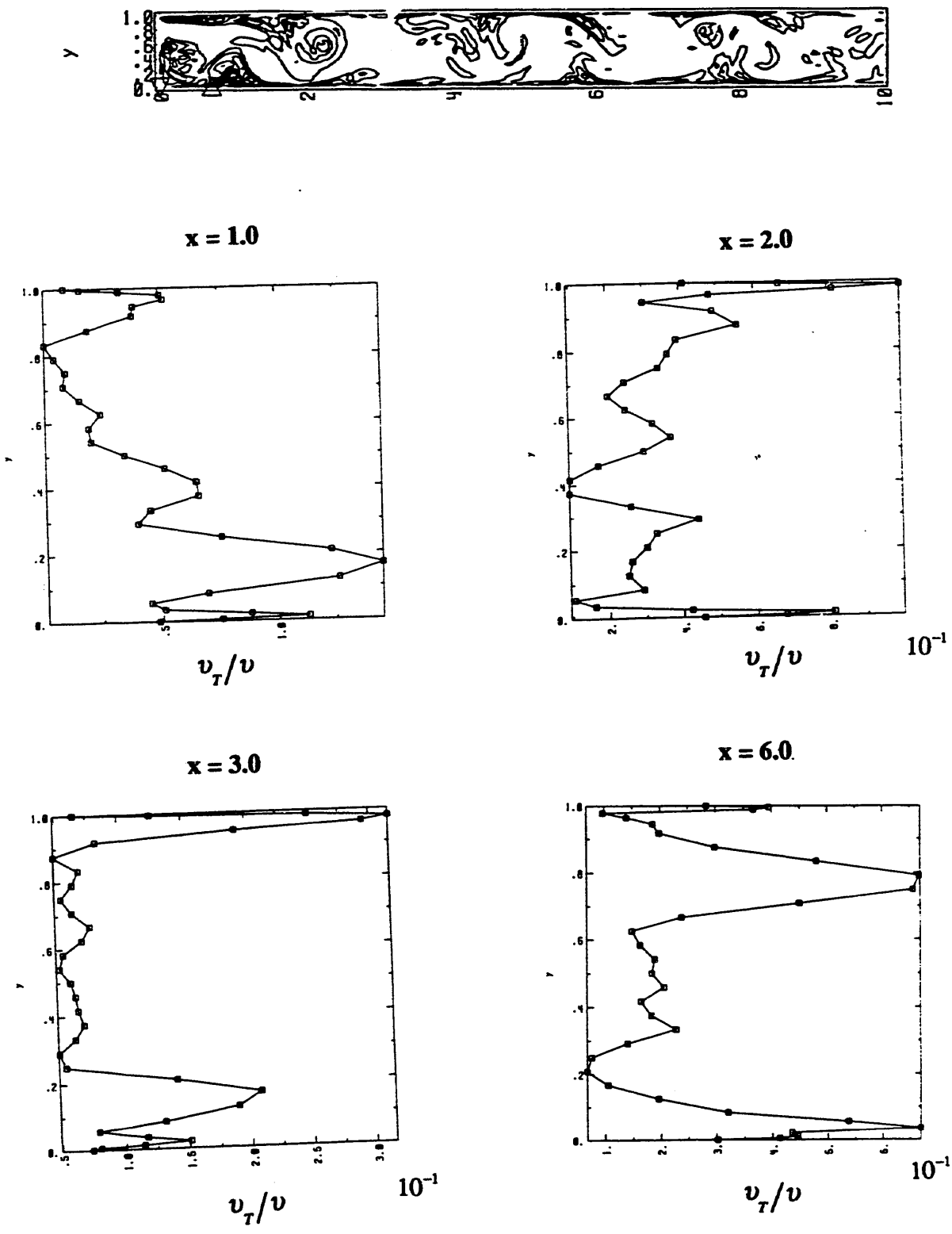

Fig 6. A υ_T contour plot and corresponding profile plots at selected locations downstream of the step.

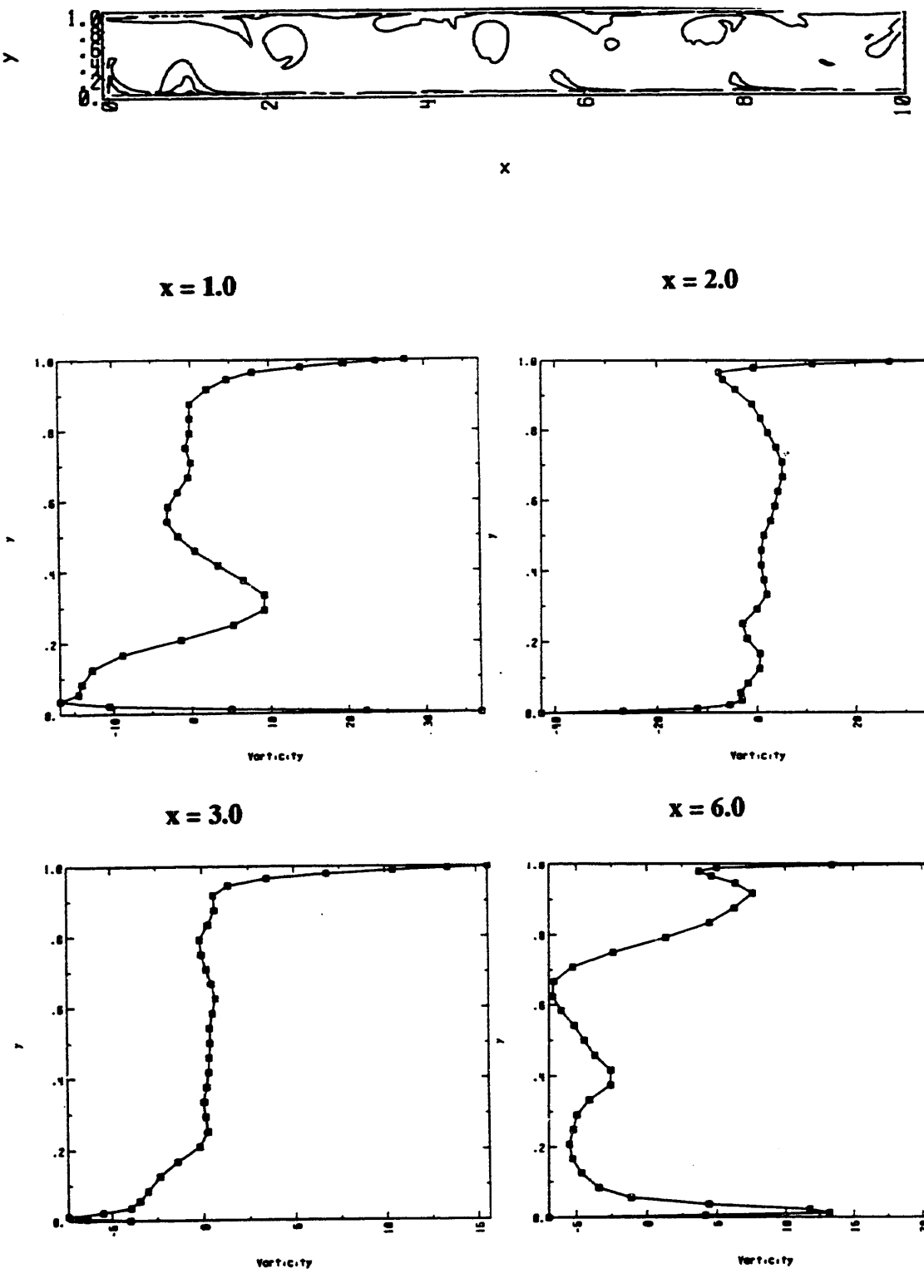

Fig 7. Vorticity contour plot and corresponding profile plots at selected locations downstream of the step.

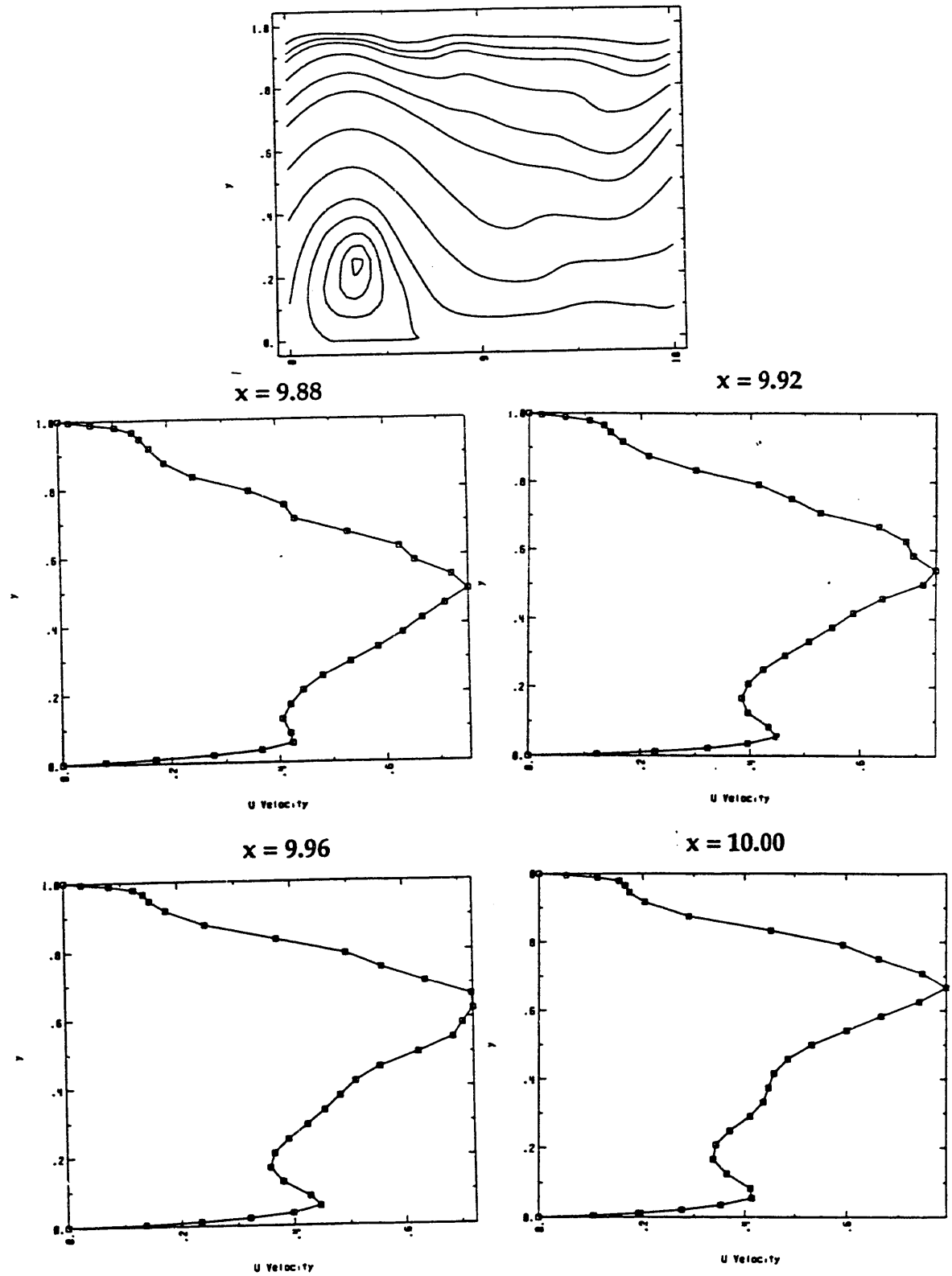

Fig. 8. The LES $\overline{u}_1$ profiles at the channel outlet for the shown stream function snapshot.

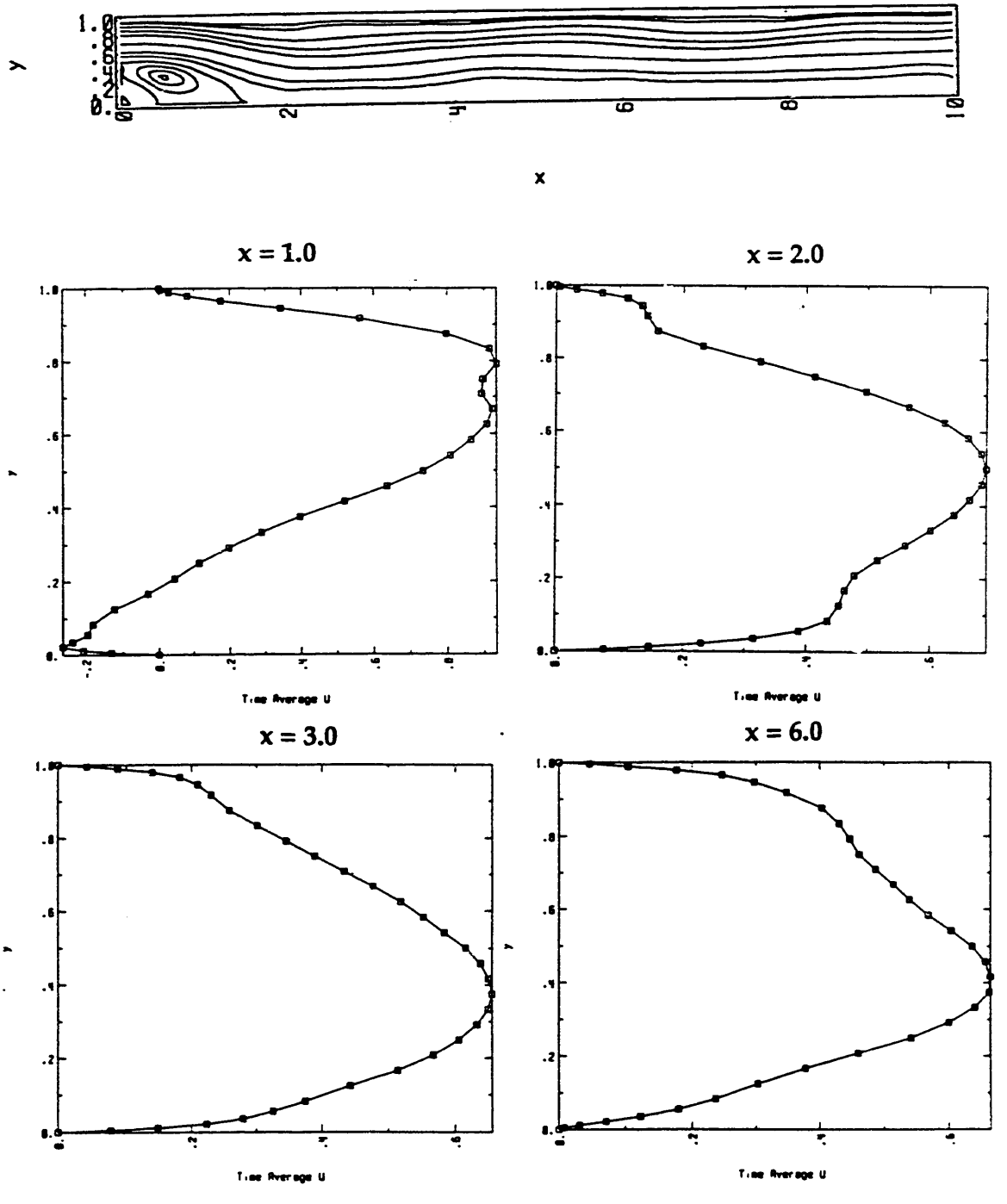

Fig. 9. The LES time-averaged $\overline{u_1}$ profiles at selected locations and the stream function plot for the time-averaged velocity.

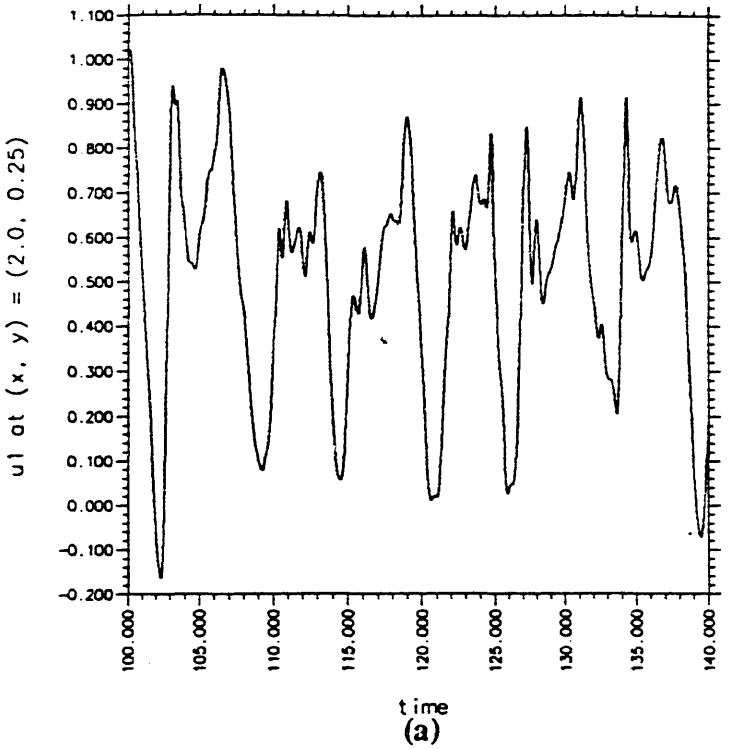

(a)

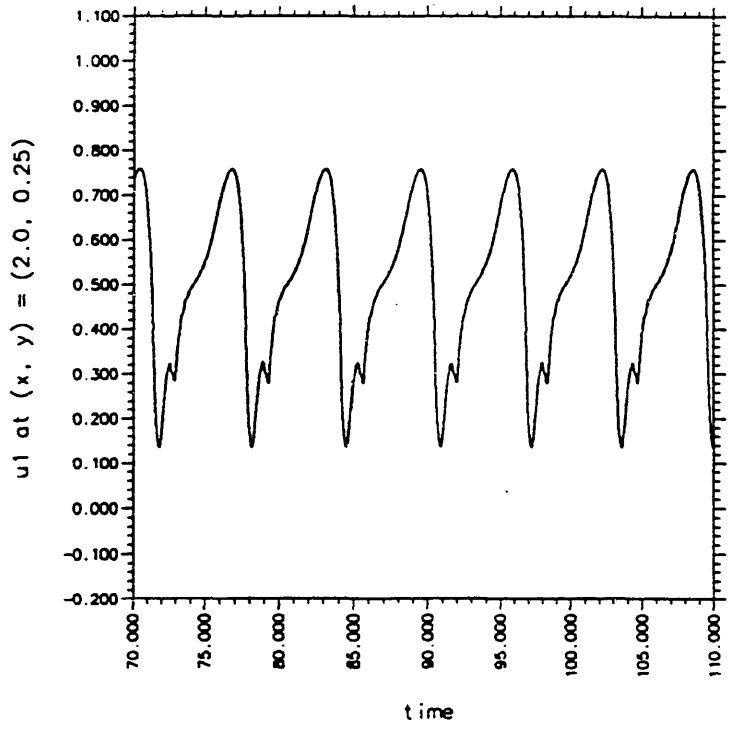

(b)

Fig. 10. Time histories of $\overline{u_1}$ at $(x_1, x_2) = (2.0, 0.25)$ for a) a DNS with the 32x244 mesh and b) the DNS with the 100x1000 mesh.

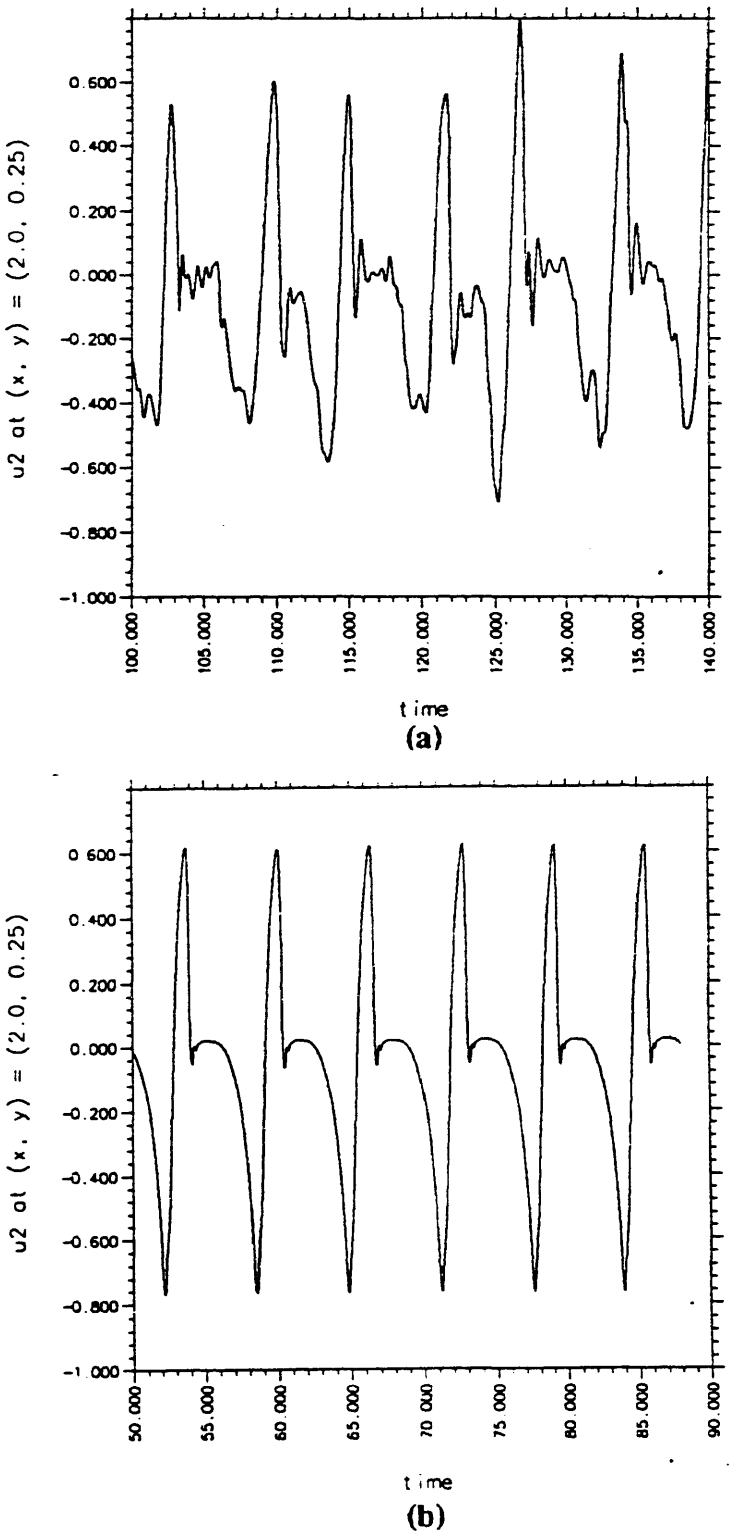

Fig. 11. Time histories of $\overline{u_2}$ at $(x_1, x_2) = (2.0, 0.25)$ for a) a DNS with the 32x244 mesh and b) the DNS with the 100x1000 mesh.

DATE
FILMED
5/4/94
END